Journal of
Applied
Crystallography

ISSN 1600-5767

Received 1 August 2014
Accepted 3 September 2014

CREDO: a new general-purpose laboratory instrument for small-angle X-ray scattering

András Wacha, Zoltán Varga and Attila Bóta*

Research Centre for Natural Sciences, Hungarian Academy of Sciences, Magyar Tudósok körútja 2, Budapest, Hungary. Correspondence e-mail: bota.attila@ttk.mta.hu

The details of a newly constructed small-angle X-ray scattering instrument are presented. The geometry of the instrument is highly customizable, enabling it to address vastly different experimental situations from academic research to industrial problems. The high degree of motorization and automation compared to conventional laboratory-scale SAXS instruments facilitates the alignment and daily use. Data reduction routines are incorporated in the instrument control software, yielding fully corrected and calibrated results promptly after the end of measurements. Optimization of the flux *versus* resolution balance can be done routinely for each measurement task. A wide, continuous range of $q = 4\pi \sin\theta/\lambda$ can be reached, from below 0.02 nm^{-1} up to 30 nm^{-1}, corresponding to periodic distances of *ca* 350 nm down to 0.2 nm. A few representative results obtained from samples of different research fields demonstrate the versatility of the instrument. Scattering curves are routinely calibrated into absolute units using a glassy carbon secondary standard. More information and recent developments can be found on the web page of the instrument at http://credo.ttk.mta.hu.

1. Introduction

The beginnings of small-angle X-ray scattering (SAXS) reach back to the first half of the 20th century (Krishnamurti, 1930; Guinier, 1937). Since then, the parallel development of theory and instrumentation up to the present day has made it possible for the method to become important and indispensable in structural studies on the nanometre scale (Guinier & Fournet, 1955; Glatter, 1982; Feigin & Svergun, 1987). While today SAXS instrumentation can be found at almost all synchrotron sources (Haubold *et al.*, 1989; Bösecke & Diat, 1997; Narayanan *et al.*, 2001; Urban *et al.*, 2003), some research groups decide to implement local measurement facilities, in order to shorten feedback times and obtain better availability.

Nowadays several companies offer operation-ready instruments. Kratky-type instruments feature a small footprint and a very compact design. Although these were traditionally slit-collimated cameras, the Kratky collimation block has been extended to allow for a point-collimated beam. The X-rays are usually focused onto the detector plane in order to reach very small scattering angles. The source-to-detector distance is usually fixed by the focal distance of the X-ray source. This type of instrument is a good choice for isotropic scatterers, such as suspensions of nanoparticles or protein solutions. Kratky-type instruments include the MICROcalix of Hecus/Bruker AXS, the SAXSpace from Anton Paar and the BioSAXS-2000 product from Rigaku.

Pinhole cameras are more flexible than Kratky-type ones but require more laboratory space. They operate usually with parallel beams and achieve the same resolution (defined by the lowest attainable scattering angle) over a much longer sample-to-detector distance. Here the full azimuthal range can be covered, enabling the study of anisotropy. Because of their larger size, these systems usually come with more spacious sample chambers, and thus a wider variety of *in situ* environments may be accommodated. The variable sample-to-detector distance enables the adaptation of the resolved q range to the current scientific needs. Synchrotron SAXS beamlines usually follow this construction pattern because of its flexibility. Commercially available pinhole cameras include the NanoSTAR from Bruker AXS, the Xeuss instrument from Xenocs and SMAX-3000 from Rigaku.

Apart from commercially available solutions, some research groups opt for custom-made laboratory SAXS instruments (Huxley *et al.*, 1965; Huxley & Brown, 1967; Kratky & Stabinger, 1984; Jakob *et al.*, 2003; Zemb *et al.*, 2003*a*,*b*). While the construction of a new SAXS beamline from the ground up can be a demanding job, the resulting instrument is usually better tuned to the problems of its users.

In this paper we present CREDO (Creative Research Equipment for DiffractiOn), a newly constructed SAXS instrument, and describe the considerations and design principles leading to its fully functional form.

2. Design considerations

The main model for our instrument was the now decommissioned B1 instrument (formerly known as JUSIFA of the Research Centre Jülich) of HASYLAB, DESY, Germany

(Haubold *et al.*, 1989; Goerigk, 2006; Vainio *et al.*, 2009). Other ideas were also taken from beamline ID02 of the European Synchrotron Radiation Facility, Grenoble, France (Urban *et al.*, 2003), and the SAXS instrument of Helmholtz-Zentrum Berlin, Germany (Hoell *et al.*, 2007).

During the planning of the new apparatus, we aimed to retain the highest possible level of variability and versatility, *i.e.* to impose as few limits in the construction as possible, facilitating future improvements, while also making it possible to optimize the instrument for every scientific problem. This case-by-case optimization means that the balance between X-ray flux and resolution (lowest value of $q = 4\pi \sin\theta/\lambda$, where 2θ is the scattering angle and λ is the X-ray wavelength) can and has to be found for each scientific problem; thus the potential of the apparatus can be fully utilized.

Another key aspect, the ease of alignment and use, is ensured by a modular construction and more extensive motorization compared to conventional laboratory SAXS systems. A fully automated and user-friendly control and data reduction software environment also facilitates daily usage.

The structural parts of the apparatus that may come into contact with X-rays were made from aluminium, brass or different polymers. Iron, steel and similar materials producing strong fluorescent X-rays upon Cu $K\alpha$ irradiation were avoided to reduce background scattering. For similar reasons, the number of windows the X-ray passes through is also reduced; in the default setup the instrument features a full vacuum system from the exit of the source to the front of the detector.

The instrument is designed with mainly transmission mode SAXS in mind, but reflection mode measurements, such as GISAXS, are also feasible.

3. Hardware setup

Each of the beamline components, *i.e.* the X-ray source, pinhole collimation stages, sample chamber, beamstop stage and detector, are mounted on the same 6095 mm-long X95 optical rail (Qioptiq GmbH, Germany) by quick-fastening holders. This construction provides the modularity and variability of the instrument while also facilitating the setup and alignment procedures. The individual components are detailed below.

3.1. X-ray source

Parallel and highly monochromatic X-rays are generated by a GeniX^{3D} Cu ULD beam delivery system with integrated FOX3D parabolic multilayer optics and a 30 W microfocus Cu anode X-ray tube (Xenocs SA, Sassenage, France). This source has a relatively high flux (>10^8 photons per second total output) and very low divergence (<0.4 mrad HW20%M both horizontally and vertically). The stability of the flux and position of the beam makes a monitor counter unnecessary for our case.

3.2. Collimation

The X-ray beam entering the camera through a 25 µm-thick Kapton window is collimated by three pinhole stages. The distances of the pinhole stages can be varied by inserting different numbers of ISO-KF DN25 flanged aluminium tubes of various lengths between them, which is a quick, easy and vacuum-proof solution. Each of the motorized pinhole holders accommodates five Pt–Ir pinhole discs of 4 mm diameter and 0.2 mm thickness (manufactured by Plano GmbH, Germany). The aperture diameters range from 150 to 1250 µm, and the currently used pinhole can be chosen by the vertical motor. An advanced calculator tool aiding the user in the choice of pinholes and pinhole distances is implemented in the instrument control software, using similar algorithms to those described in the work of Pedersen (2004).

3.3. Two-dimensional position-sensitive detector

X-rays are detected with a Pilatus 300K two-dimensional CMOS hybrid pixel detector (Dectris Ltd, Switzerland) (Henrich *et al.*, 2009; Kraft *et al.*, 2009; Donath *et al.*, 2013). It is widely used in both laboratory-scale and synchrotron beamlines, because of its low background, zero noise, high linearity and dynamic range, low point spread, and effectively zero maintenance. It has a sensitive area of 83.8 × 106.5 mm and can tolerate more than 2×10^6 X-rays per second in each pixel.

3.4. Sample stage

The sample environment consists of a vacuum chamber (21 × 29 × 29 cm inner dimensions), with a motorized platform inserted from above (*cf.* Fig. 1). The horizontal and vertical stroke lengths are 35 and 75 mm, respectively, which, along with the large volume of the chamber, enables the accommodation of different sample holders and environments. Signal or material input to the chamber is feasible through special purpose flanges.

Standard sample holders include a ladder mounting for solid or powder samples (films, plates *etc.*, currently up to 14 pieces), a temperature-controlling block for capillaries (currently up to five pieces) up to approximately 1.6 mm diameter, and a holder for a single capillary with the option of applying a static magnetic field of 0.7 T.

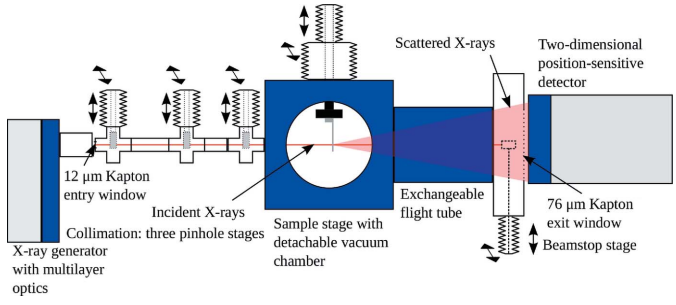

Figure 1
Schematic layout of CREDO.

The vacuum chamber may also be removed. This enables the measurement of non-vacuum-tolerant samples and *in situ* sample environments (*i.e.* a shear cell), at the price of two more Kapton windows in the beam and increased air scattering.

3.5. Flight path

In order to be able to cover different ranges of q, different numbers of tubes made of poly(vinyl chloride) (15 cm inner diameter and 4 mm wall thickness) can be mounted after the sample stage. This material was chosen because of its high linear absorption coefficient (8.0 mm^{-1} for Cu $K\alpha$ photons), its availability and the lack of fluorescent elements.

The vacuum level of the full flight path is usually around 0.02 mbar and is constantly monitored using a TPG-201-type Pirani gauge (Pfeiffer Vacuum Technology AG, Germany) mounted on the beamstop stage.

As the detector cannot be placed in vacuum, a sheet of 76 µm-thick KaptonX foil ends the flight path. Taking advantage of the ~3 mm inter-module gaps of the Pilatus detector, the window is supported by two horizontal nickel-plated brass slats of the same thickness.

At the end of the flight tube, just before the window, an XY-motorized beamstop stage is installed. Beamstops of various size, shape and opacity can be mounted on a thin vertical bronze wire of 1 mm diameter.

3.6. Motion control

The instrument is equipped with ten stepper motors, driven by TMCM-351 and TMCM-6110 integrated stepper motor controller and driver boards from Trinamic Ltd (Hamburg, Germany). These boards provide high-level accurate motor control and are able to drive three (TMCM-351) or six (TMCM-6110) axes simultaneously. Communication between the boards and the instrument control computer is done through RS-232 and USB interfaces, using the Trinamic Motion Control Language (TMCL).

All stepper motors are mounted outside the evacuated space. Movement is transferred inside using edge-welded membrane bellows (COMVAT AG, Haag, Switzerland).

4. Instrument control software and data reduction

The instrument control software (*SAXSCtrl*) is written in the Python scripting language. The program features an intuitive easy-to-use graphical user interface. All the devices mentioned above, *i.e.* the X-ray source, the detector, all ten stepper motors, the Pirani gauge and, optionally, a temperature-controlling water circulator, can be accessed and controlled. Because of its stability and reliability, Linux was chosen as the underlying platform, but the software can be ported to other operating systems with little effort.

Scattering patterns recorded by the detector are saved by its *camserver* software as CBF files (Bernstein & Hammersley, 2005). Data reduction is carried out promptly after each exposure using a standard algorithm, which consists of normalization (measurement time, transmission, sample thickness), background subtraction and correction for geometrical distortions (solid angle of image elements, angle dependence of self-absorption). Intensities are also scaled into absolute scattering cross-section units of $cm^{-1}\,sr^{-1}$, using a pre-calibrated 1 mm-thick glassy carbon specimen as a secondary reference (Zhang *et al.*, 2010). Calibration of the abscissa from pixel values to q is done using silver behenate (Huang *et al.*, 1993). The instrument control software relies strongly on *Numpy*, a Python package for matrix computations (Oliphant, 2007), and *matplotlib*, a package for high-quality plotting (Hunter, 2007). Fully corrected two-dimensional images are written currently as NPZ files (default binary format of *Numpy*) and in the widely accepted NeXuS format (Könnecke, 2006).

Sample transmissions are measured with the two-dimensional detector in the low-power (9 W) mode of the X-ray tube, by moving the beamstop out of the beam.

For the alignment of the instrument, *i.e.* positioning the pinholes, the beamstop and the sample stage, scans can also be performed with respect to one of the stepper motors. These measurements are usually done using a low-power beam. Instead of using other counters, different parts of the Pilatus 300K detector area can be selected by mask matrices and thus act as virtual detectors by defining a mathematical operation on the unmasked pixels. The software is also capable of two-dimensional scans (*i.e.* 'mapping') by employing two stepper motors.

A simple scripting language was implemented for *SAXSCtrl*, which enables unattended automatic operation. Apart from standard instrument control commands, such as X-ray generator power setting, sample change, motor movement, temperature selection and exposure with the detector, the user can define variables, evaluate simple mathematical expressions and use these as input for almost all commands. Flow control is implemented using labels and conditional or unconditional goto statements.

5. Representative results

5.1. Calibration standards

Fig. 2 presents the scattering curves of two commonly used calibrant materials measured by the CREDO instrument. Silver behenate (AgBeh) is routinely used as a secondary calibrant for the q scale (Binnemans *et al.*, 2004). The periodicity of our AgBeh sample was determined to be 5.840 (4) nm by measuring the sample at multiple sample-to-detector distances and determining the distance differences to a high accuracy. Glassy carbon is a widely accepted standard for the calibration of scattering curves into absolute units of scattering cross section. Several glassy carbon standards suitable for different energy ranges have been used at JUSIFA since 1987 (Materials from SGL CARBON AG, Werk Ringsdorff, Bonn, Germany) (Haubold *et al.*, 1989; Dietz, 1991; Buth, 1992; Fan *et al.*, 2010). It features a relatively long plateau in its scattering pattern, which makes the scaling

procedure more stable. Our specimen was obtained from Dr Jan Ilavsky (APS, Argonne National Laboratories, Chicago, USA) with the corresponding calibration data.

The scattering curves presented in Fig. 2 were measured using three sample-to-detector distances: 1578.3 mm (long distance), 454.6 mm (short distance) and 72.6 mm (wide-angle X-ray scattering). The resulting data were scaled and merged together in order to yield curves spanning an exceptionally broad range in both q (0.019–29.87 nm^{-1}, corresponding to 320.2 and 0.21 nm, respectively) and absolute intensity (more than eight orders of magnitude in the case of silver behenate).

5.2. Silica nanoparticles

SAXS is a useful and straightforward means to determine the size distribution of relatively monodisperse nanoparticles. Fig. 3 shows the characteristic SAXS curves from three SiO_2 nanoparticle suspensions: two in-house prepared samples, synthesized by the method of Hartlen *et al.* (2008), and additionally one commercially available sample (Klebosol 30R50, AZ Electronic Materials France SAS, courtesy of Gert Roebben, Institute of Reference Materials and Measurements, Joint Research Centre of the European Commission, Geel, Belgium).

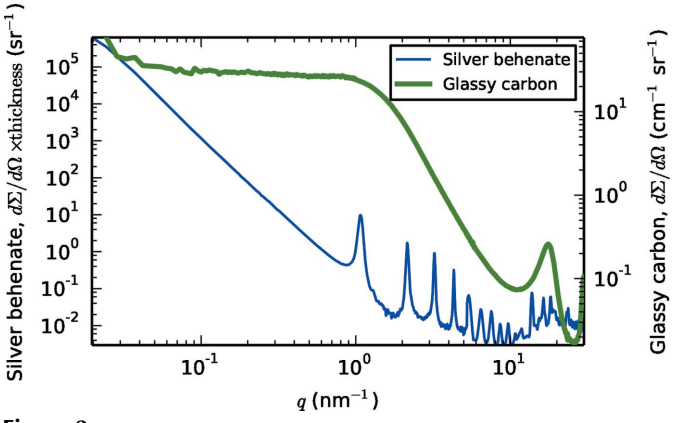

Figure 2
Measured SAXS curves of common calibrant materials.

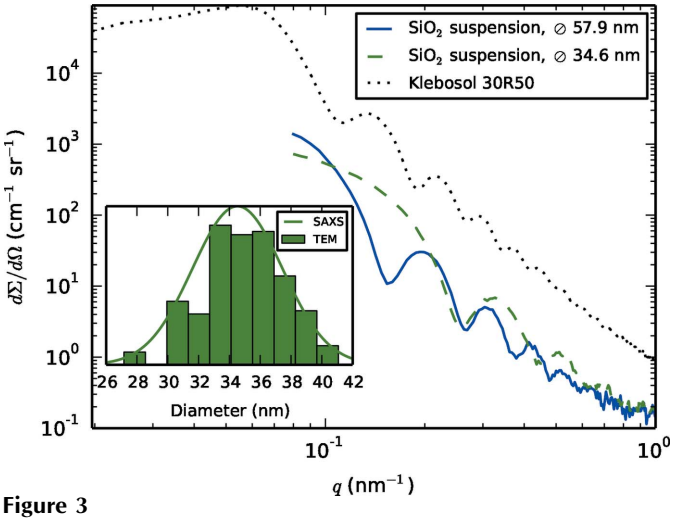

Figure 3
Measured SAXS curves of SiO_2 suspensions. The inset shows the size distribution determined from the SAXS curve and a histogram of particle diameters found by analysing transmission electron micrographs for the second SiO_2 suspension with *ca* 34.6 nm diameter.

These results demonstrate well the average form factor of an ensemble of nearly monodisperse spherical particles. Scattering curves for the two smaller diameter silicas (continuous and dashed lines in Fig. 3) start with a Guinier range characteristic of the radius of gyration in particulate systems. After this the oscillatory Fourier range follows, which enables a more accurate determination of the size distribution of the particles. The scattering pattern ends with the Porod range with the characteristic q^{-4} slope.

The dotted line in Fig. 3 corresponds to the commercial silica. Its larger size (*ca* 82.4 nm diameter) means that a smaller q range has to be reached in order to resolve the Guinier range. The low-q part of the scattering curve is distorted by concentration effects.

The size distributions of these nanoparticle ensembles were also determined from transmission electron micrographs, and good agreement was found between the two methods, as shown in the inset of Fig. 3 for the case of the smaller in-house prepared SiO_2 suspension.

5.3. Sterically stabilized phospholipid vesicles

Self-assembled phospholipid structures are of great scientific importance for several reasons. They not only are good model systems for biological (cell) membranes (Pabst *et al.*, 2010), but serve as important drug delivery vehicles (Chang & Yeh, 2011), and can be used as reaction volume confinements in nanoparticle synthesis (Bóta *et al.*, 2007*a*). Spherical phospholipid vesicles (liposomes), especially their unilamellar forms, are frequently studied by our research group (Bóta *et al.*, 2007*b*; Varga *et al.*, 2008, 2010). Fig. 4 presents the background-corrected SAXS curve of a sterically stabilized liposome system prepared in our laboratory (Varga *et al.*, 2012). It represents the scattering factor of the phospholipid bilayer and the PEG molecules ensuring steric stability.

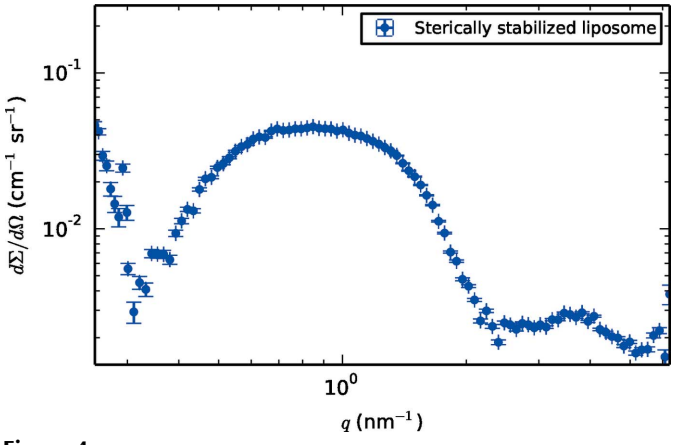

Figure 4
Small-angle X-ray scattering curve of a sterically stabilized liposome.

Table 1
Summary of characteristics.

Quantity	Value
Lowest attainable q	<0.02 nm^{-1}
Highest resolvable periodic distance ($2\pi/q_{min}$)	>320 nm
Largest radius of gyration	>50 nm
Highest attainable q	29.9 nm^{-1}
Highest attainable scattering angle (2θ)	33°
Lowest resolvable periodic distance	0.2 nm
Typical flux at sample (⊘ 0.7 mm beam, medium q)	165 000 photons per second
Typical beamstop size	⊘ 4 mm
Typical sample-to-detector distances	72, 454, 1500 mm
Inherent beam divergence of the source	<0.4 mrad HW20%M
Beam spectral purity	<0.5% Cu $K\beta$ contamination
Flux variation	<0.1% over 18 h

Table 2
Typical measurement times.

Material and measurement conditions	Typical exposure time
Silver behenate for sample-to-detector distance calibration	<1 min
Glassy carbon for absolute intensity calibration	∼1–2 min
Bilayer form factor of a sterically stabilized phospholipid vesicle (10 mg ml^{-1})	∼2–3 h
Radius of gyration from a 10 mg ml^{-1} solution of bovine serum albumin	∼1 h
SAXS measurements on SiO_2 nanoparticle samples in solution	∼1–2 h
SAXS measurements on nanoparticle samples in powder state	∼1 min

6. Conclusion

A new general purpose large laboratory instrument, an efficient and highly flexible system for small-angle X-ray scattering, has been constructed. Its main characteristics are collected in Table 1. Typical measurement times for common samples under different experimental conditions are presented in Table 2.

The demonstrated versatility of CREDO provides scattering data with nearly the same quality as obtainable at synchrotron beamlines. The resulting curves, scaled into absolute differential scattering cross-section units, obtained on different samples at CREDO and at synchrotron SAXS beamlines (not shown in this paper) prove the reliability of our design. It must also be mentioned that the moderate flux of the source reduces the measurement possibilities. This disadvantage, however, can be improved by applying new types of X-ray sources, as was done in the case of GALAXI, which was recently constructed at the Jülich Research Centre (Forschungszentrum Jülich, Germany).

Our plans for upgrading the CREDO apparatus in the future include a more powerful X-ray source (based on the newly developed metal-jet technology) and the possibility to use lower-wavelength radiation instead of or beside Cu $K\alpha$, which would extend the scattering range to smaller dimensions (higher q) and allow the measurement of more highly absorbing samples, such as metal alloys or ceramics.

Further details and actual news of the instrument are to be found on its web page at http://credo.ttk.mta.hu.

The facility was realized through the cooperation of the Research Centre for Natural Sciences of the Hungarian Academy of Sciences and Gedeon Richter Plc (Dr Ádám Demeter, Dr Zsolt Szombathelyi and Dr György Thaler, to whom the authors are greatly indebted), co-funded by a project of the Hungarian National Scientific Research Fund (grant No. CNK 81052) of the Hungarian National Innovation Office and by a grant from the Central Hungarian Operative Program (KMOP-1.1.2-07/1-2008-0002). The authors would also like to express their gratitude towards Marcell Pálmai for the SiO_2 nanoparticles, Gert Roebben (IRMM, JRC) for the Klebosol sample, Ferenc Laufer (FeriTex Ltd) for the mechanical work, Dr Jan Ilavsky (APS) for the calibrated glassy carbon specimen, and Dr Ulla Vainio, Dr Guenter Goerigk, Dr Armin Hoell, Dr Michael Krumrey and Dr Christian Gollwitzer for the experience gained at synchrotron beamlines at DESY and BESSY. The authors of this work are not associated in any way with the companies/industries of the mentioned instruments. Product names in this paper are used only for the sake of clarity, without any intent to endorse any particular product or company. Trademarks mentioned are the properties of their respective owners.

References

Bernstein, H. J. & Hammersley, A. P. (2005). *International Tables for Crystallography*, Vol. G, *Definition and Exchange of Crystallographic Data*, edited by S. R. Hall & B. McMahon, pp. 37–43. Heidelberg: Springer.
Binnemans, K., Van Deun, R., Thijs, B., Vanwelkenhuysen, I. & Geuens, I. (2004). *Chem. Mater.* **16**, 2021–2027.
Bösecke, P. & Diat, O. (1997). *J. Appl. Cryst.* **30**, 867–871.
Bóta, A., Varga, Z. & Goerigk, G. (2007*a*). *J. Phys. Chem. B*, **111**, 1911–1915.
Bóta, A., Varga, Z. & Goerigk, G. (2007*b*). *J. Appl. Cryst.* **40**(Suppl.), s259–s263.
Buth, G. W. (1992). PhD thesis, Rheinisch-Westfaelische Technische Hochschule Aachen University, Aachen, Germany.
Chang, H.-I. & Yeh, M.-K. (2011). *Int. J. Nanomed.* **2012:7**, 49–60.
Dietz, V. (1991). PhD thesis, Rheinisch-Westfaelische Technische Hochschule Aachen University, Aachen, Germany.
Donath, T., Brandstetter, S., Cibik, L., Commichau, S., Hofer, P., Krumrey, M., Lüthi, B., Marggraf, S., Müller, P., Schneebeli, M., Schulze-Briese, C. & Wernecke, J. (2013). *J. Phys. Conf. Ser.* **425**, 062001.
Fan, L., Degen, M., Bendle, S., Grupido, N. & Ilavsky, J. (2010). *J. Phys. Conf. Ser.* **247**, 012005.
Feigin, L. A. & Svergun, D. I. (1987). *Structure Analysis by Small-Angle X-ray and Neutron Scattering*. New York: Plenum Press.
Glatter, O. & Kratky, O. (1982). *Small Angle X-ray Scattering*. New York: Academic Press.
Goerigk, G. (2006). Annual Report, HASYLAB Hamburg, Germany, pp. 77–78.
Guinier, A. (1937). *C. R. Hebd. Séances Acad. Sci.* **204**, 1115.
Guinier, A. & Fournet, G. (1955). *Small-Angle Scattering of X-rays*. New York: John Wiley and Sons.
Hartlen, K. D., Athanasopoulos, A. P. T. & Kitaev, V. (2008). *Langmuir*, **24**, 1714–1720.

Haubold, H. G., Gruenhagen, K., Wagener, M., Jungbluth, H., Heer, H., Pfeil, A., Rongen, H., Brandenberg, G., Moeller, R. & Matzerath, J. (1989). *Rev. Sci. Instrum.* **60**, 1943–1946.
Henrich, B., Bergamaschi, A., Broennimann, C., Dinapoli, R., Eikenberry, E. F., Johnson, I., Kobas, M., Kraft, P., Mozzanica, A. & Schmitt, B. (2009). *Nucl. Instrum. Methods Phys. Res. Sect. A*, **607**, 247–249.
Hoell, A., Zizak, I., Bieder, H. & Mokrani, L. (2007). Patent No. DE 102006029449.
Huang, T. C., Toraya, H., Blanton, T. N. & Wu, Y. (1993). *J. Appl. Cryst.* **26**, 180–184.
Hunter, J. D. (2007). *Comput. Sci. Eng.* **9**, 90–95.
Huxley, H. E. & Brown, W. (1967). *J. Mol. Biol.* **30**, 383.
Huxley, H. E., Brown, W. & Holmes, K. C. (1965). *Nature*, **206**, 1358.
Jakob, H. F., Erlacher, K. & Fratzl, P. (2003). *Mater. Sci. Forum*, **414–415**, 411–418.
Könnecke, M. (2006). *Physica B*, **385–386**, 1343–1345.
Kraft, P., Bergamaschi, A., Broennimann, Ch., Dinapoli, R., Eikenberry, E. F., Henrich, B., Johnson, I., Mozzanica, A., Schlepütz, C. M., Willmott, P. R. & Schmitt, B. (2009). *J. Synchrotron Rad.* **16**, 368–375.
Kratky, O. & Stabinger, H. (1984). *Colloid Polym. Sci.* **262**, 345–360.
Krishnamurti, P. (1930). *Indian J. Phys.* **5**, 473–486.
Narayanan, T., Diat, O. & Boesecke, P. (2001). *Nucl. Instrum. Methods Phys. Res. Sect. A*, **467**, 1005–1009.
Oliphant, T. E. (2007). *Comput. Sci. Eng.* **9**, 10–20.
Pabst, G., Kučerka, N., Nieh, M.-P., Rheinstädter, M. C. & Katsaras, J. (2010). *Chem. Phys. Lipids*, **163**, 460–479.
Pedersen, J. S. (2004). *J. Appl. Cryst.* **37**, 369–380.
Urban, V., Panine, P., Ponchut, C., Boesecke, P. & Narayanan, T. (2003). *J. Appl. Cryst.* **36**, 809–811.
Vainio, U., Schubert, T., Botta, S., Blume, J., Wacha, A., Lohmann, M., Kracht, T. & Gehrke, R. (2009). Annual Report, HASYLAB, Hamburg, Germany.
Varga, Z., Berényi, S., Szokol, B., Õrfi, L., Kéri, G., Peták, I., Hoell, A. & Bóta, A. (2010). *J. Phys. Chem. B*, **114**, 6850–6854.
Varga, Z., Bóta, A. & Goerigk, G. (2008). *J. Phys. Chem. B*, **112**, 8430–8433.
Varga, Z., Wacha, A., Vainio, U., Gummel, J. & Bóta, A. (2012). *Chem. Phys. Lipids*, **165**, 387–392.
Zemb, T., Taché, O., Né, F. & Spalla, O. (2003*a*). *Rev. Sci. Instrum.* **74**, 2456–2462.
Zemb, T., Tache, O., Né, F. & Spalla, O. (2003*b*). *J. Appl. Cryst.* **36**, 800–805.
Zhang, F., Ilavsky, J., Long, G. G., Quintana, J. P. G., Allen, A. J. & Jemian, P. R. (2010). *Metall. Mater. Trans. A*, **41**, 1151–1158.